50 MeV Cyclotron Development

P. Miller, W.S. Chien, D. Gossman, H. Hilbert, W. Harder, D. Johnson,
D. Magistro, M. Mallory, J.F.P. Marchand, and G. Stork

1. Internal Beam Phase Probe

Our direct-excitation phase probe[1] has been the means for improving the isochronism of the cyclotron for several beams required for experiments during the last year: 5.5 and 7.5 MeV $^{1}H^{+}$, 16-25 MeV $^{2}H^{+}$, 27, 73 and 76 MeV $^{3}He^{2+}$, 19 MeV $^{3}He^{1+}$, 6.2 and 8.2 MeV $^{3}He^{1+}$. In many of these cases the gamma ray time-of-flight technique will not work due to its energy threshold. The $^{3}He^{1+}$ beam is being used for studying (^{3}He,n) reactions and is also a cyclotron analogue for the much-used heavy ion $^{12}C^{4+}$. The phase curves for this beam measured before and after adjustment of the trim coils are shown in Fig. 1. The appearance of sharp turn structure in the probe trace of Fig. 2 is a manifestation of the reduction of beam energy spread effected by the field trimming procedure.

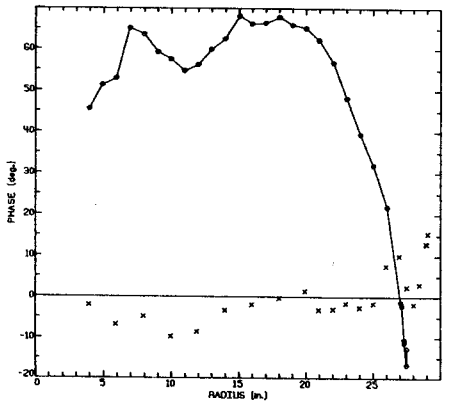

Fig. 1.--Measured phase curves for the 19 MeV $^{3}He^{1+}$ beam. Open circles represent the original settings; crosses show the effect of applying corrections to the trim coils.

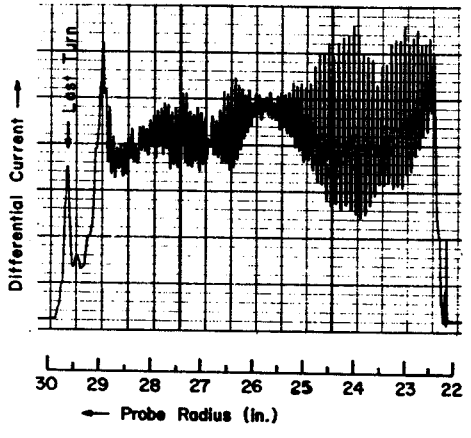

Fig. 2.--Radial scan of differential probe showing turn structure in the 77 MeV $^{12}C^{4+}$ beam out to extraction. The source slit was 0.38 mm wide; a single 0.38 mm wide phase selecting slit was inserted into the beam on the 28th turn. The beam current was 300 enA

2. Heavy Ion Acceleration

During the last year a large number of heavy ion beams were successfully accelerated on the cyclotron. Table I is a list of the heavy ion beams that have been accelerated, with the maximum energy and intensity (at exit of cyclotron) for each. These beam intensities are comparable with those measured at Oak Ridge and Berkeley cyclotrons.

Table I. MSU Heavy Ion Beams.

Ion	Max. Energy (MeV)	Observed External Intensity (eμA)
$^{6}Li^{3+}$	75	1.0 - 0.2
$^{7}Li^{3+}$	74	0.1
$^{6}Li^{2+}$	38	3
$^{9}Be^{4+}$	103	$>10^{5}$ part/sec+
$^{11}B^{4+}$	85	20enA
$^{12}C^{4+}$	77	10
$^{12}C^{3+}$	36	20
$^{12}C^{5+}$	120	15enA
$^{13}C^{4+}$	70	3enA*
$^{14}N^{5+}$	103	3
$^{16}O^{6+}$	130	0.5 - 0.05
$^{16}O^{5+}$	90	1.0
$^{20}Ne^{5+}$	60	1.0
$^{40}Ar^{8+}$	92	30enA

*Source feed CO gas with natural isotope abundance

+Source feed solid charge of beryllium copper (2% Be).

A unique feature of the heavy ion source is the capability to change the cathodes in a short time (Fig. 3). Another feature is an all solid state power supply (except for pass tube) leading to greater reliability. A dual gas system to allow mixing a small amount of Xe with the arc support gas has increased the beam intensity and improved the arc stability for oxygen and lithium beams. Use of the heavy ion source has required improvements in the cooling of the cyclotron accelerating slits (puller), since the beam power dissipated from heavy ions is larger than for light ions. A water line has been attached to the puller. This decreased the rf sparking somewhat. The ion source slit width was also reduced from 3.5 to 1.5 mm to reduce the beam power dissipated in the central region of the cyclotron.

The average lifetime of the ion source has been dissappointing low (~2-3 hrs.). Usually the arc becomes extinguished and cannot be restruck (open circuit). The short-circuit failure mode is observed less frequently. One feature of this ion source is that the cathode high voltage circuit is directly exposed to the rf voltage on the dee.

Therefore a fluctuation in the cyclotron rf may cause the source to drop out. Secondly, the most desired beam (i.e. Li^{3+} -- the intensity now being achieved was thought impossible a year ago) requires the ion source to be run right at its critical gas flow, therefore making it vulnerable to fluctuations. A source modification, recognizing these experimental desires and operating experiences is under design.

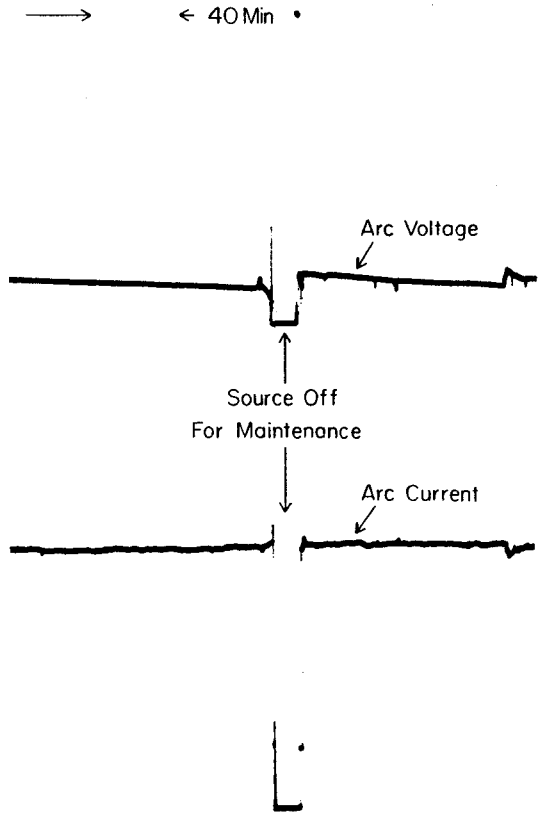

Fig. 3.--Plot of arc current (upper trace) and arc voltage (lower trace) showing the time required to clean the source, replace the necessary parts and resume operations. Typical down time is 25 minutes. The two cathodes are used once and discarded. The copper chimney is replaced with a cleaned one in a rotation cycle, as is the tantalum end cover on the source.

3. Electrostatic Deflector Improvements

Since Feb. 1977 we have used spark anodes (ground planes) made of titanium instead of the tungsten. The maximum potential difference attainable and the lifetime before maintenance is required have not been noticeably affected by this change. Titanium is so much cheaper than tungsten that it is practical to use the plates just once, whereas the tungsten plates were normally polished and cleaned for reuse a number of times. Titanium is more susceptible to burn-out than tungsten . On two occasions, when an insulator also failed and there were many sparks in a short time, the titanium was found to have melted. The excessive heating may have been caused primarily by local electron bombardment (dark current).

The lifetime of the deflector surfaces appears to be controlled by the number of vacuum break/pump-down cycles experienced. An attempt to rejuvenate a contaminated deflector by glow discharge cleaning using argon gas was apparently successful and seemed to extend the life of the deflector about one month. The breakdown of an insulator at that time, rather than the condition of the sparking plates forced disassembly of the deflector for repairs. The parameters of the cleaning cycle were based on experience with vacuum conditioning of storage rings at CERN.[2]

The discharge was run for 1 hr at a current of .1 to .15 A to get more than 10^{18} ions/cm^2 over the 2000 cm^2 surface. The arc was maintained by a 300V DC power supply and a 10^3 Ω series stabilizing resistor. The deflector electrode potential was positive 160 V with respect to ground. The pressure in the deflector region was not measured, but a gauge at the opposite side of the cyclotron (near the pump) read 200 μ (.2 torr). Pure argon gas was flowed continuously during the cleaning cycle. More recently we have had success in restoring a deflector to good condition using hydrogen in the arc and alternating current. This technique has been used at the Berkeley cyclotron.[3]

4. Computer Controls

The microprocessor-based control system for the cyclotron field trimming coils was installed in Nov. 1976, replacing a control system using motor-operated potentionmeters. In 8 months of continuous use there has been only one failure of the computer, requiring restarting of the program. There were also several instances of intermittent loss of regulation of the current in one coil (no.6), which has been overcome by suppressing noise picked up from external sources.

The system has 12 bits of precision for setting the reference signal to each power supply. A 3 digit display indicates this value to the operator, who can make manual settings either with a knob (connected to an incremental encoder) or with a thumbwheel switch. For each control channel there is a module containing these elements on the console. We plan to extend the system to other operator controlled power supplies within the next year, specifically harmonic coils, deflector, magnetic channel, steering magnets and quadrupole magnets. A total of 32 control channels will be provided, of which 29 are dedicated to existing equipment as described above.

The microprocessor is linked to the PDP 11/20 cyclotron computer for program modification and supporting computations in case control functions requiring simultaneous variation of several power supplies required. An example is to change the energy dispersion of the beam on target, preserving the focus and the magnification, which would require

changing the current in several quadrupoles. The present system therefore allows one of the unused control channels to become a dispersion control by so programming the computers.

Another project receiving attention is automatic centering of the cyclotron beam. A program for the PDP 11/20 has been worked out which runs the probe inside the cyclotron to take a radial turn profile, locates the turns and fits their positions. An example of the graphical display by the computer of such a scan with the fit is shown in Fig. 4. In this case the beam is centered (to within 0.008 in.), so the turn spacing monotonically decreases with radius. A typical pattern for a moderately off-center beam is shown in Fig. 5., and for a large centering error in Fig. 6. In the latter case about 20% of the turns do not appear on the probe scan because the precession of the particle orbit carries it closer to the center of the cyclotron than an earlier turn. The program is not yet able to automatically arrive at corrections in this circumstance. It will center the beam quickly if all turns appear on the probe trace, as in Fig. 5.

---

1. P. Miller, W.S. Chien, J.F.P. Marchand, BAPS 21, (1976) 988.
2. Ultrahigh Vacuum Technology for Storage Rings, by Ehrhard Fisher, to be published in IEEE Transactions on Nucl. Sci., June 1977 (1977 Particle Accelerator Conf. Proceedings).
3. Bob H. Smith and Herman A. Grunder, Lawrence Berkeley Lab. Report UCLR-10654 (March 1963).

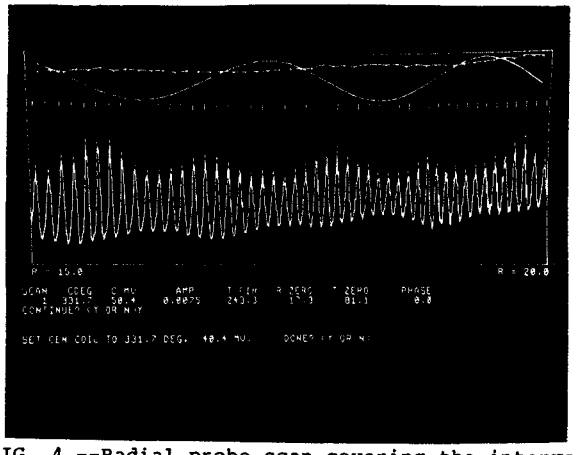

FIG. 4.--Radial probe scan covering the interval R=15 inches to 20 inches for a centered proton beam with extraction energy of 42 MeV.

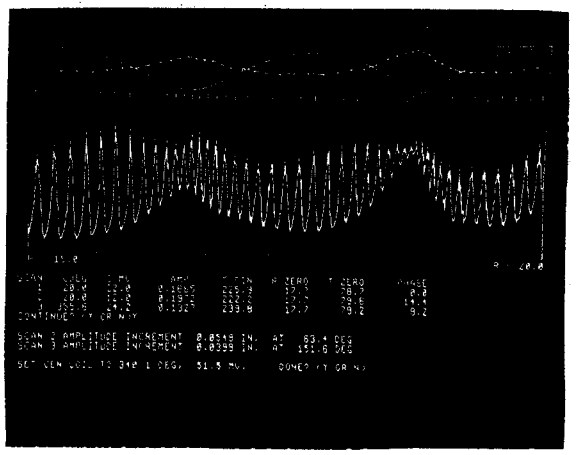

FIG. 5.--Same as Fig. 4, except current in the inner harmonic coils has been changed, resulting in a centering error of 3.3mm(.13 inches).

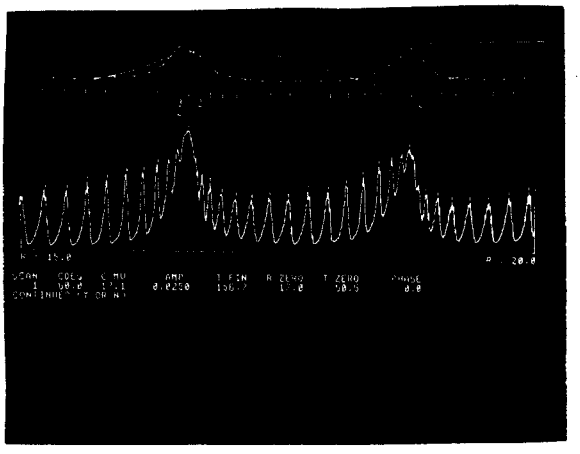

FIG. 6.--Same as Fig. 5, except a larger centering error has been produced. Some turns "loop back" inside the orbit of previous turns. These turns do not appear on the probe scan, since the probe completely intercepts the beam.

Multiwire Counter Development for the Split Pole Spectrograph

R.G. Markham, R. Melin

In the last annual report we described a multiwire-drift counter which we were considering for use in the split pole spectrograph. Its primary characteristics would be its ability to measure angle of incidence and time of arrival as well as accurately determine position. This would give us the ability to correct the energy loss and time-of-flight information for their dependence on particle trajectory, and it would allow us to use larger solid angles with good resolution by making aberration corrections.

During this report year we have completed the detector and electronics design, and we have carried out computer studies of the time derivation and aberration correction problems. These are reported below.

a) THE DESIGN

The readout scheme is essentially as was previously described. The guard wires, now two between each active wire, are to be connected to successive taps on a low impedance delay line composed of nine dual-in-line potted delay lines of ten taps each. This packaged design is compact and makes for easy replacement in the event that a delay line is damaged by high voltage. The active wires will be parallel connected in a repeating sequence of five with each of the five being fed to a low impedance preamplifier and constant fraction time discriminator of "homemade" design. The wires will be spaced 1.91 mm apart for a total length of 51.4 cm for 90 active wires.

The counter depth was chosen to be 2.54 cm so that for a 4 ms aperture valid events must fire at least three and no more than five active wires. This will ensure that enough wires are involved to reconstruct the event and that no active readout line will have signals from two wires.

The mechanical construction is shown in Fig.1.

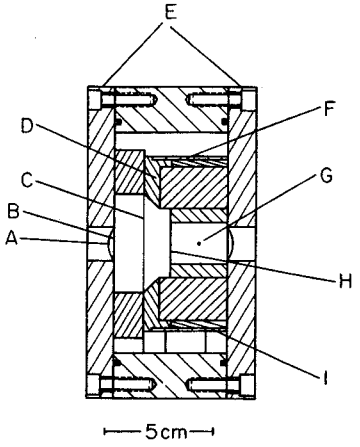

Fig. 1.-Counter parts are: A. front window, B. front foil, C. wire plane, D. wire support, F. active wire matrix board, G. anode wire for ΔE counter, H. separator foil, I. guard wire-delay line board.

The gas box is closed on the front and back with heavy cover plates to increase its rigidity and gas retaining foils can either be adhered to these plates or extended out to the edges of the box. Additional foils (which serve to maintain uniform fields) are located at the front and back of the multiwire chamber. The wires themselves are terminated on circuit boards at the top and bottom and are stretched over spacer blocks which are scored to maintain the wire spacing. The top board is also a matrix board connecting the active wires to successive readout lines, and the lower board connects the guard wires to the delay line chips. The remainder of the electronics -- preamps and bias networks -- are located at one end of the counter. Structural strength is derived by the use of stainless steel bars with end supports. At the back of the counter, between the bars is located a single wire proportional counter whose sole purpose is to provide energy loss information.

b) COMPUTER STUDY OF LEADING EDGE AND CONSTANT FRACTION TIMING FOR A MULTIWIRE COUNTER

In conjunction with the design of the multiwire proportional counter, a study was done to determine the effect of random ionization on the time resolution of the counter. This is crucial since the spatial localization is done by drift time thus causing the spatial resolution to be directly proportional to the time resolution.

The geometry of the counter for which these calculations was done consists of a plane of wires lying between parallel grounded foil planes. The plane of wires is made up of active wires separated by pairs of guard wires. If the guard and active wires are appropriately biased and the parallel planes are grounded, the electric field is that of a periodic array of identical wires and the solution is analytic. Electrons produced in this region will be accelerated towards the nearest wire and their trajectories will be the electric field lines because the frequent collisions with gas molecules will cause the electrons to be continually redirected -- also at high enough fields they will drift with a terminal velocity. These collisions also may release additional electrons so that the original electrons multiply as they move towards the wire, but this avalanche develops only very near the wire.

In calculating the trajectories of the electrons the time required for an electron, starting at any position in the region, to drift to the wire may be found. Once the drift time as a function of position was known the particle track was divided up into equal time of arrival lengths. A track at 45° to the wire plane (and at some distance from the wire considered) was studied. Figure 2 shows percent of ionization path vs. arrival

time if equal sized time-of-arrival bins are used. Notice that the charge from a large fraction of the particle track would arrive within a few nanosecond period but that charge would drift in for a considerable length of time afterwards. This is a consequence of the 45° angle of incidence.

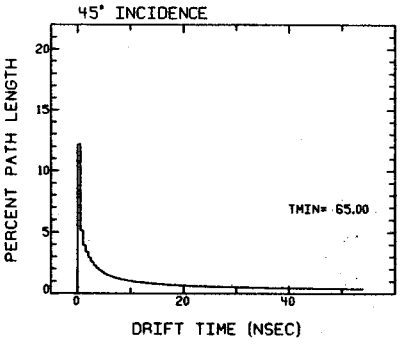

FIG. 2.--Shows the fractions of a 45° particle track that correspond to different times of arrival. This can be envisioned by considering the portions of the particle track that are within a small range of distance along the field lines from the wire. These distance ranges correspond to the different arrival time bins.

Once the equal time bins had been established, the ionization in each of these bins may be calculated and then the time development of the pulse may be simulated. The ionization was calculated by randomizing the energy losses along the particle track in each of these bins using a random number generator having a Blunk-Liesgang frequency distribution.[1] This distribution is an empirical fit to data for minimum ionizing particles and seems to be well suited to the 35-150 MeV protons and similar energy alphas for which these calculations were done. The time development of the pulse can be found by calculating the growth of the avalanche due to the ionization from each path length bin arriving at its respective time. The avalanche development was approximated by the Wilkinson form[2] which is a logarithmic growth in time of the ionization as a result of the collisions of the drift electrons with those of the gas. Once the time development of the pulse is known the time development for the pulse which is integrated and differentiated can be simulated. By recreating many such pulses, time and pulse-height spectra are generated.

The time resolution for leading edge and constant fraction timing was calculated, with the results for no shaping appearing in Table I.

Table I. Time and spatial resolution for LEADING EDGE and CONSTANT FRACTION timing.

Fraction	LEADING EDGE FWHM(n sec)	LEADING EDGE FWHM(μm)	CONSTANT FRACTION FWHM(nsec)	CONSTANT FRACTION FWHM(μm)
.02	1.3	52	1.2	50.
.05	2.5	100	1.5	60.
.10	4.3	185	2.0	80.
.25	--	--	2.8	110.
.50	28.8	1150	4.4	190.

It appears that constant fraction timing is the better of the two methods in this application in that it is less affected by jitter in the timing due to the random ionization along the path length. This fluctuation has a large effect on the rise time of the pulse and some effect on the pulse height. The differences in the rise have a substantial effect on leading edge timing whereas constant fraction timing makes some use of correlation of the rise time with the pulse height to reduce the uncertainty. The resolution for the constant fraction timing is also not as dependent on the fraction chosen as is the leading edge timing on the level chosen.

c) ABERRATION CORRECTIONS FOR THE SPLIT POLE SPECTROGRAPH

In order to judge how effectively we might be able to compensate for spectrograph aberrations, a computer simulation code was written. Aberrations to third order were used and the detector was assumed to have finite horizontal and vertical position resolution as well as finite angle resolution. A linear relation between spectrograph entrance angle and focal plane incidence angle was used. All other parameters including aperture size were made part of the input.

The procedure was to divide the entrance aperture into a 100 by 100 grid and with due account taken of the symmetry, this was then reduced to a 100 by 50 grid on one side of the median plane. Each point on the grid represents a value of θ and ϕ which are the angles, with respect to the central ray, in and out of the median plane. For each grid point, the point of intersection of the ray with the focal plane was computed using the expressions:

$$Y-Y_{\text{central ray}} = A\cdot\phi^2 + B\cdot\theta^3 + C\cdot\theta\cdot\phi^2 + D\cdot\theta^2 \quad (1)$$

$$Z-Z_{\text{central ray}} = E\cdot\theta\cdot\phi \quad (2)$$

where Y is in the direction of dispersion and Z is normal to the median plane. To simulate the detector performance a "measured" value of θ is picked as a random number with a gaussian distribution about the true value of θ for that grid point. If the absolute value of this "measured" θ came out to be greater than two standard deviations from zero then the B and D terms in equation (1) were subtracted using the measured θ.

The procedure for removing the ϕ aberrations was to pick a "measured" value of Z as was done for θ and then calculate ϕ from equation (2) also using the "measured" value of θ. If the "measured" Z was large enough, then the A and C terms were subtracted from equation (1) again using the "measured" values.

This left us with a Y position corrected for aberrations as well as the detector could. To also account for finite detector resolution a gaussian distributed random number was added to this value of Y. Finally a position spectrum was formed from

the Y values of each grid point.

Figure 3 shows a corrected and uncorrected peak shape using the parameters of Table II and a rectangular aperture $(\Delta\theta,\Delta\phi) = (\pm 3^{o}, \pm 1^{o})$. Notice the uncorrected spectrum has wings extending out beyond the ±2 mm limits of the plot. These wings are totally removed by the correction procedure, but the full width at half maximum of the peak is not improved. The peak width is about 0.4 mm FWHM which is due to an assumed detector resolution 0.25 mm FWHM and the remaining 0.3 mm due to uncorrected aberrations which are mostly ϕ^2 and $\theta\phi^2$ terms. For small apertures aberration corrections are less valuable -- unless one has extremely good θ and ϕ resolution. This can be seen by inspecting the criteria used to decide whether or not to correct a particular event. The criteria is: if the uncertainty in the correction is larger than the correction itself, don't correct. For small apertures one has small corrections only and few events can be corrected. Hence for small apertures one remains aberration limited.

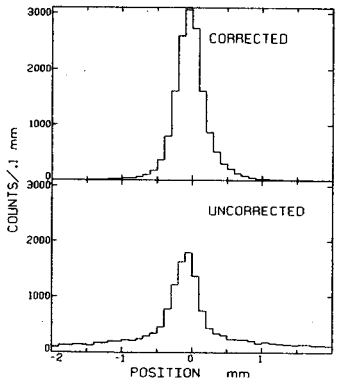

Figure 3.

Table II. Input Parameters

A	-1000	mm/r^2
B	-17000	mm/r^3
C	1000	mm/r^3
D	200	mm/r^2
E	-8000	mm/r^2
σ counter	0.1	mm rms
σ_Z	0.6	mm rms
σ_θ	0.2	deg rms

As expected the ϕ aberrations are the largest for square apertures and the scheme used to make these corrections is not very effective. At best only rays going into the corners of these apertures can be corrected; hence, one might just as well use ones that are oval shaped and not try to correct for ϕ aberrations. A larger θ opening can be used to regain the lost solid angle.

1. P.V. Ramana Murthy and G.D. Demeester, Nucl. Instr. and Meth. 56 (1967) 93.
2. Wilkinson, D.M., Ionization Chambers and Counters (The University Press, Cambridge, 1950).

Development of a Short High Resolution Delay Line Counter

R.C. Melin, R.G.H. Robertson, and J.A. Nolen

In our program to build a high resolution counter to be used in the Enge split pole for optimizing the beam quality, various attempts were made to build thin charge division counters.[1] Detectors constructed for normally incident particles were built having thicknesses of 1 to 2 mm and a length of 1 cm. Position resolution of 50 μm with a 1 mm thick detector has been obtained. The charge division counters utilized carbon coated quartz wires which were susceptible to deterioration and to resistance changes with age and usage. In order to alleviate this problem a different type of readout was needed. Such a readout which had been used in some of the larger detectors at MSU is the delay-line readout.[2] The delay line consists of an anode wire which lies above a plane of pick-up stripes. The pickup stripes have charge induced on them as the avalanche nears the anode wire. Each of these pickup stripes is connected to the next by a delay element which adds a known time delay to the signal. The position is measured by using a signal from one end to start a TAC and a delayed signal from the other end of the delay line to stop the TAC. The previous delay lines used have pickup stripes at 45° to the anode wires to correspond to the trajectory of the particles through the detector. The present detector was designed for normal incidence and to be 1 cm long and 2 mm thick. The short delay line uses a printed circuit board to hold the DIP lumped constant delay line, with the pickup stripes evaporated onto the printed board making contact with the taps from the delay line. The pickup stripes were made by evaporating copper into the board masked by an array of wires in a vacuum evaporator. This allowed the stripes to be made with .25-mm spacings between the .75-mm wide stripes. The evaporator shadowing technique makes very uniform lines with definite edges which is difficult to achieve on this size scale with standard etching techniques. The copper on the printed board and the evaporated copper was then tin plated using standard techniques to make the board more permanent. The delay line of 100 ns total delay with ten taps was made in the form of a standard 14 pin DIP by Data Delay Devices Inc.

The printed circuit board with delay line was attached to a Delrin block which was milled to form a bridge for the .0125-mm anode wire and to support the .00625-mm havar foil which defines the back surface of the detector. The Delrin block is mounted in an aluminum block which forms the gas-tight box. An entrance aperture 10 mm long and 2.2 mm high with a .0625-mm aluminized mylar window defines the front of the detector. Electrical signals are fed through the aluminum box by a 9 pin kovar seal O-ringed into the box. The back of the aluminum box has a .0625-mm aluminized mylar window to allow particles to pass through a surface barrier detector for particle identification.

Tests of the detector were made with an alpha source with 5 slits, and with 35 MeV protons elastically scattered incident normally on the detector (see Figures). Results show the line width for protons elastically scattered from ^{12}C to be 85 μm FWHM for both short quartz wire charge division counter and short delay line. Tests show that the short delay-line counters have comparable resolution with a noticeable increase in durability. The delay line also has the advantage of producing fast signals suitable for timing.

1. R.C. Melin, J.A. Nolen and R.G. Markham, MSU Annual Reports 1974-76, p. 115.
2. R.G. Markham, R.G.H. Robertson, Nucl. Instr. and Meth. 129, 131(1975).

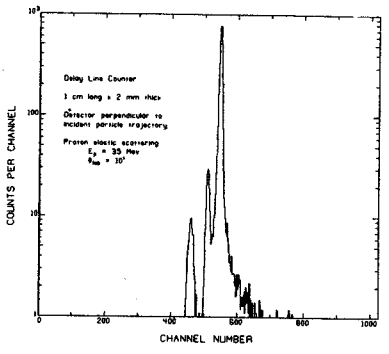

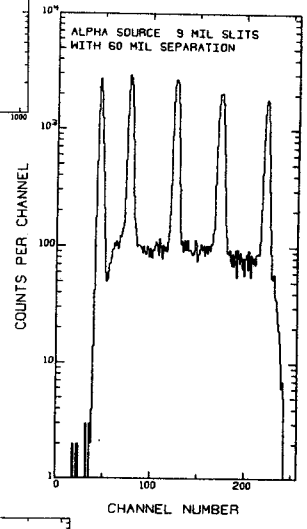

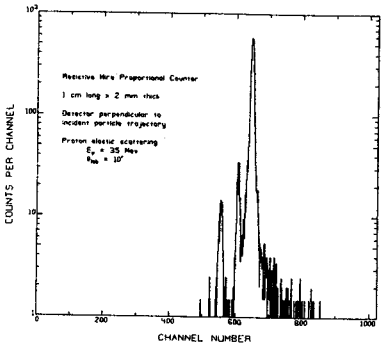

Electrostatic Deflector for the Enge Split-Pole Spectrograph

R.G.H. Robertson

The addition of an electrostatic deflector to the spectrograph has extended our capabilities for precision mass measurements and the study of low-cross-section reactions in the presence of intense backgrounds. The deflector consists of two $\frac{1}{2}$" aluminum plates with radiused edges, spaced $1\frac{1}{2}$" apart by means of porcelain insulators. It is supported by three posts which stand on the floor of the vacuum chamber between the first and second poles of the magnet. Figure 1 shows the shape of the plates and their location in the magnet. The shape is intended to provide uniform deflection along the focal plane, in the approximation that the focal plane is at the vertical focal point of the second dipole.

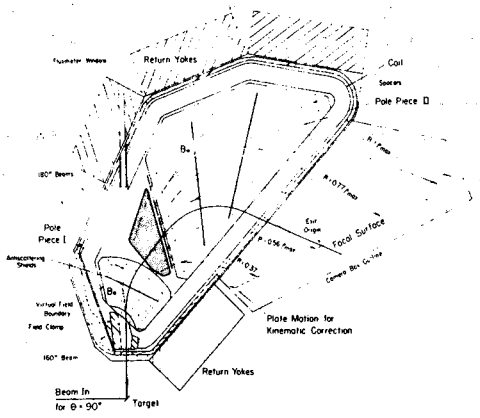

Fig. 1.-Location of the deflector (stippled area) in the split-pole spectrograph.

The plates are driven by a 20-kV low-current supply, and the potential is brought into the spectrograph through a fitting in a lucite plate which replaces the normal iron blank-off plate in the side of the spectrograph. The deflection at the hi-ρ end of the focal plane in millimeters is approximately

$$d = 10 \frac{Vq}{E}$$

where V is the voltage on the plates, q the charge on the ion and E the energy. For particles of the same magnetic rigidity, the deflection is proportional to $\frac{m}{q}$, where m is the mass of the ion.

The deflector is useful in two different experimental situations. First, it permits the use of nuclear emulsions even for reactions with very low cross-sections. Hence the precision mass measurement techniques developed by Nolen at MSU can be extended to previously unfeasible reactions. A measurement of the Q-value for the $^{14}C(p,t)^{12}C(T=2)$ reaction, with a cross section of a few $\mu b\ sr^{-1}$, has successfully been completed (described elsewhere in this report). A test must still be made, however, to learn if the deflector introduces a centroid shift. Another reaction being studied with this technique is $^{12}C(^{3}He, ^{6}He)^{9}C$. The ^{6}He tracks can be easily separated and scanned despite the intense flux of protons, deuterons and alphas on the focal plane. Of course, it is not possible to separate tritons from ^{6}He electrostatically, but the triton background is weak and the tracks much fainter than ^{6}He tracks.

The second application of the deflector is with live detectors in the focal plane. A short mask is placed over the entrance window of the detector. It is then possible to deflect intense particle groups onto the mask while allowing the groups of interest (with different $\frac{m}{q}$) into the detector. Kashy and collaborators have used this technique to advantage in a search for the $^{58}Ni(^{12}C, ^{13}B)^{57}Cu$ reaction (described elsewhere in this report).

Response of Pilot B Scintillator to Heavy Ions

A. Ledebuhr, D. Mueller, E. Kashy and W. Benenson

As the light output from organic scintillators is frequently used as a means of particle identification, a better understanding of the relationship between a particle's energy and its light output is needed. A measurement of this relationship for most of the ions lighter than A=17 was made using the Cyclotron at Michigan State University.

The experimental procedure was to have a beam at fixed energy bombard a target positioned in the scattering chamber of the Enge spectrograph. The large variety of particles coming from this target was then used to excite a scintillator placed in the focal plane. This is more convenient than accelerating each type of ion separately as other investigators in this area have done.[1,2] In addition, the light output from such beta unstable ions as ^{8}Li or ^{12}B could be observed with this method.

The detector set up was as follows: A 5 cm long position sensitive gas proportional counter was placed in the focal plane of the spectrograph. This was followed by a 5 cm long, 1 cm square piece of Pilot B Scintillator placed directly on the face of a photomultiplier (P.M.) tube. The proportional counter, which was necessary for particle identification, decreased the energy of the particles striking the scintillator, and corrections for this energy loss were made using the program DERMOL.[3]

Of greatest concern in this experiment was the possibility that at the high magnetic fields used in the spectrograph a decrease in the gain of the P.M. tube would affect the light output data. To avoid this problem, 1 MeV electrons from the decay of ^{207}Bi served as a calibration for the light output. By measuring the electrons' light output at each new field of the spectrograph and by dividing all the particles' light output by this value, any changes in the phototube gain would not affect the relative light output of the ions. This also eliminated any normalization problems from various amplifier gain settings and biasing voltages used in the P.M. tube for the different fields in the spectrograph. At the highest fields, the pulses produced by the electrons were half as large as at zero magnetic field.

In the first run we used a 75 MeV ^{3}He beam and obtained data for the following ions, with energies up to 80 MeV Z^2/A:

protons, deuterons, tritons, ^{3}He, alphas, ^{6}He, ^{6}Li, ^{7}Li, ^{7}Be, ^{9}Be, ^{10}Be

In our second run we used 100 MeV ^{14}N on ^{12}C, ^{27}Al, and ^{9}Be targets, obtaining data for the following ions with energies up to 36 MeV Z^2/A:

^{6}Li, ^{7}Li, ^{8}Li, ^{7}Be, ^{9}Be, ^{10}Be, ^{10}B, ^{11}B, ^{12}B, ^{11}C, ^{12}C, ^{13}C, ^{14}C, ^{13}N, ^{14}N, ^{15}N, ^{16}N, ^{15}O, ^{16}O, ^{17}O

A preliminary analysis of relative light output vs. magnetic rigidity curves shows qualitative agreement with Becchetti's results.[1] A further analysis of this data is currently in progress.

---

1. F.D. Becchetti, C.E. Thorn, and M.J. Levine, Response of Plastic Scintillator Detectors to Heavy Ions, Z<35, E<170 MeV, Nuclear Inst. Meth. 138, 93-104(1976).
2. M. Buenerd, et al., Response of Pilot U Scintillator to Heavy Ions, Nuclear Inst. Meth. 136, 173-177(1976).
3. P.S. Miller, Program DERMOL, MSU Computer Library, Jan. 25, 1973.

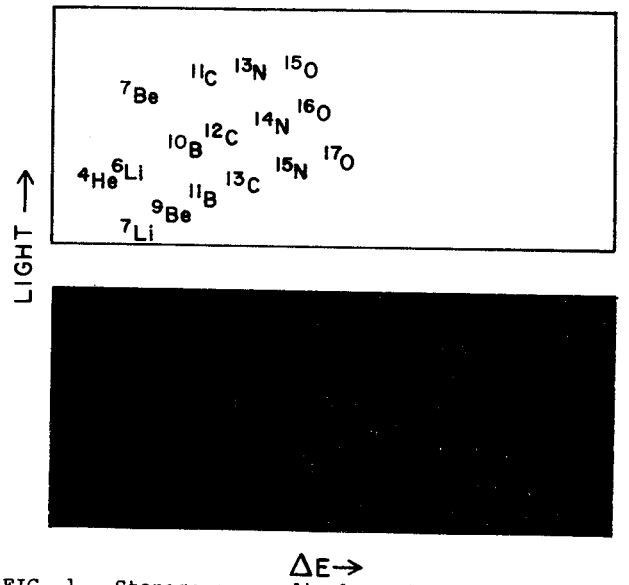

FIG. 1.--Storage scope display of light output versus energy loss in the proportional counter.

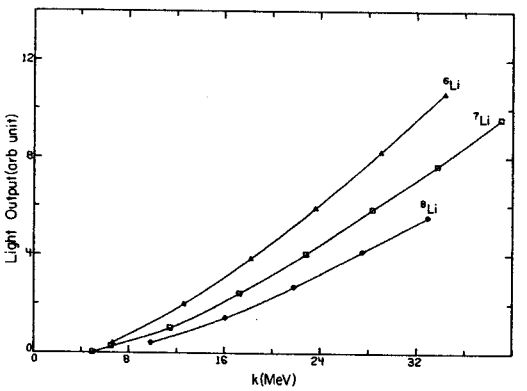

FIG. 2.--Light output versus magneti rigidity for ^{6}Li, ^{7}Li, and ^{8}Li stopped in Pilot B scintillator. Energy is given by $K \cdot Z^2/A$.

Operation of an Efficient Two Dimensional Scanner for Beta Emitters

R.G. Markham, S.M. Austin and M. Stya

In many uses of radioactive tracers, the tracer isotope is incorporated by biochemical processes into a variety of compounds and one wishes to determine the relative labelling of these compounds. Analytic techniques, such as thin layer electrophoresis, or chromatography may be used to spatially separate these compounds and their position (and the intensity of the labelling) determined by scanning from a commercial geiger counter scanner if separation in one dimension is sufficient to unambiguously separate all compounds of interest. Unfortunately, this is often not the case. In studies of the fixation of ^{13}N labelled nitrogen gas by the blue-green alga (cyanobarterium), Anabaerca Cylindrica it was necessary to distinguish a large number of amino acids among which the fixed ^{13}N was distributed. To obtain a clean separation among these it was necessary to follow thin layer electrophoresis in one direction with chromatography in an orthogonal direction. This left the labelled compounds spread in small spots on a two dimensional area with dimensions of 5 cm x 20 cm. There were no available techniques for scanning such two dimensional distributions with the required resolution (2-3 mm) and efficiency ($\sim$1%) and within a time scale consistent with the 10.0 minute half-life of ^{13}N.

In the last annual report we described a line scanner system based on position sensitive proportional counter (PSPC) techniques, including ray tracing, which had the required resolution and an efficiency $\gtrsim 0.1f$ where f is the fractional resolution required in the shortest dimension. Although this system was optimized with the ^{13}N experiment in mind it should prove useful whenever one needs to determine the location of a beta emitter (with beta energy $\gtrsim$50 keV) such as ^{14}C, ^{11}C on a flat substate with dimensions not much greater than 30 cm x 30 cm.

Briefly, this system consists of two single-wire proportional counters positioned one above the other over the horizontal surface to be scanned. Each of these counters is position sensitive by virtue of their resistive anode wire which causes the avalanche charge to flow to each end according to the inverse of the resistance from the avalanche point to that end. These charge signals are amplified, digitized and computer processed to produce two lateral positions at two distances from the surface. This information determines the lateral coordinate of the decaying nucleus. To determine the longitudinal coordinate the surface is moved at a constant speed on a scanning table beneath the counters which have a restricted longitudinal opening. When the decay is detected the position of the table is also sent to the computer and a two dimensional array element is incremented according to the location of the decay.

The system has been in use for approximately one year with the following observations. The position resolution along the counter ranges from 2 to 3 mm FWHM for an angle restriction of $\pm 30^{o}$ from the normal. This gives the counter a geometrical efficiency of 2.7% for detecting a decay directly below the entrance aperture. In practice a lower efficiency is obtained because many events lead to larger than average pulses which we choose not to process. The only background counting appears to be due to cosmic rays which give signals identical in pulse height and angle to those of the source. Because this background is small in the ^{13}N counting application, we have made no effort to eliminate the cosmic rays by standard anti-coincidence techniques.

The major failing of the device is its frequent need for maintenance. The carbon coated quartz wires lose their coating in areas of high counting. This causes position nonlinearity, lost events and eventually high voltage breakdown of the counter. The lifetime of the wires is about forty hours of use with repair taking about eight hours. We are hoping to find a simple procedure to repair the wires in place by redepositing the carbon.

A Magnet for Measuring g-Factors

S.R. Faber, L.E. Young and F.M. Bernthal

A magnet for measuring g-factors has been constructed and tested. The design followed closely that given in the previous annual report. A 5 ¼ in. diameter vacuum chamber rests between two truncated cone type pole tips forming a 1 in. gap over a 2.5 in. diameter area in which the targets lie.

The magnet has been calibrated with a flip coil. It was found to give a magnetic field that was uniform over the ½ in. diameter target area to about 1/2% with a 3% deviation over a 2 in. diameter circle. The drift and the non-reproducibility of a given magnetic field from the power supply current dial was less than 0.1%. The maximum continuous magnetic field obtained is 2.29 T at a little over 400 amperes.

A preliminary measurement of a known g-factor was done to test the system. The g-factor of the 8^+ isomer in ^{210}Po was measured using 26 MeV alphas incident on a 58 mg/cm^2 natural Pb target. The beam line setup worked quite well. The beam was bent 21° as it passed through the chamber, exited through the rear port, and was dumped about 5 feet away with no detectable structure in the time spectrum resulting from the beam dump. After 6 hours of counting the background subtracted spectrum in Fig. 1 resulted. When fit to the function $N(t)=N_o e^{\tau t}\,1+N_1 \sin(\omega_L t-\theta)$ where N_0, τ, N_1, ω_L and θ were left as unknown parameters, a frequency $\omega_L=.1613 \pm .0019$ nsec^{-1} resulted. When combined with the determination of H using the flip coil measurements, this translates to g=0.911±2% uncorrected for Knight or chemical shifts in the lead target. This result agrees with the accepted value[1] of +0.914±.001, also an uncorrected value. The two measurements are directly comparable since they were carried out in the same chemical environment.

An experiment has recently been done to measure the g-factor of the $19/2^-$ state in ^{115}Sb. The structure of this state has been proposed[2] to be $d_{5/2} \otimes {}^{114}\text{Sn}\ 7^-_{19/2^-}$. The additivity relationship, combining the g-factors of ^{114}Sn (7^-) and ^{121}Sb ($5/2^+$), implies a g-factor of 0.295 for ^{115}Sb ($19/2^-$).

The reaction was $^{115}\text{In}(\alpha,4n\gamma)^{115}\text{Sb}$ using 48 MeV alphas on a 110 mg/cm^2 natural In target. Two detectors were used, one at 135° and one at 225°. The ratio of the difference to the sum of the TAC spectra from each detector for the 1217 keV transition is shown in Figure 2. A preliminary fit to the data gives a frequency corresponding to a g-factor of +0.288.

1. O. Hausser et al. Nucl. Phys. A273,253(1976).
2. J. Bron et al., Nucl. Phys. A279,365(1977).

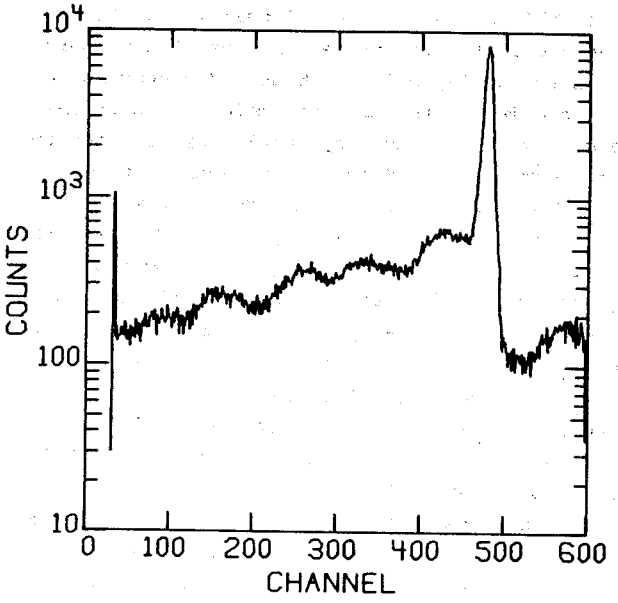

FIG. 1.--TAC spectrum of the 1180 keV line from ^{210}Po.

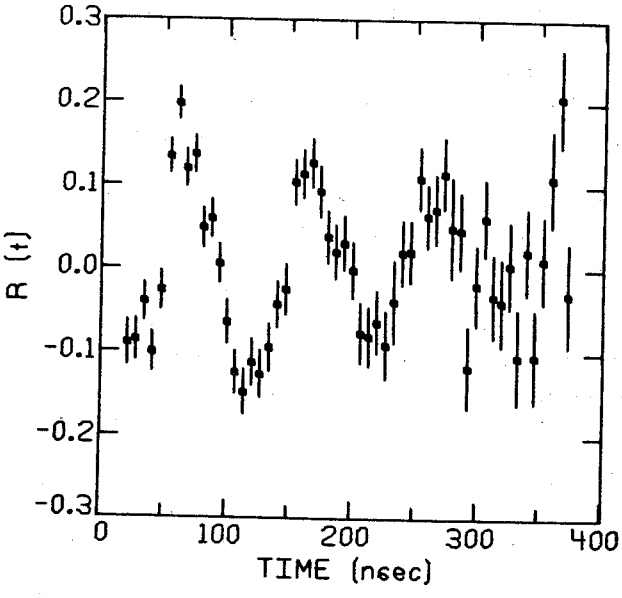

FIG. 2.--Ratio for the 1217 line in ^{115}Sb.

Calibration of a Neutron Time-of-Flight Detector for Atmospheric Neutron Measurements

A. Galonsky, L.E. Young, L. Friling,* L. Hsieh,* J.A. Lockwood,* D. Rowley,* and R. Simons*

Experimenters were stimulated to measure the neutron flux and energy spectrum at the top of the earth's atmosphere when Singer[1], and others suggested that decay of neutrons was the primary mechanism for injecting protons and electrons into the Van Allen belts. In this model the neutrons themselves are produced by cosmic-ray interactions in the atmosphere. Some of the neutrons scatter back out of the atmosphere and decay in flight.

Because of the difficulty of the measurements, the status of this "cosmic ray albedo neutron decay" theory has fluctuated. At present it is not believed capable of supplying enough protons below about 10 MeV. However, according to recent experimental results by the University of New Hampshire group[2], for example, the spectrum above 20 MeV may be in agreement with the theory. There are still discrepancies amongst experiments.

Current best experimental techniques involve the use of hydrogenous scintillators, liquid scintillators at that, thus permitting, by pulse shape discrimination, identification of neutron events as distinct from a large background of gamma-ray events. Even so, for energies above 20 MeV the efficiency of scintillators for neutron detection is difficult to compute with great accuracy because neutron-carbon interactions, whose cross sections are uncertain, become very significant relative to n-p scattering as the neutron energy increases. For this reason empirical calibrations were made here at MSU in 1975.[3] The result was almost a factor-of-two change in the atmospheric neutron spectrum between 30 and 75 MeV.[2]

For measurement of an albedo the single-scintillator method is deficient in that it lacks directionality. The present detector employs double scattering and the special kinematics of n-p scattering to select the n-p scattering events, including the incident neutron direction, while suppressing events from neutron-carbon interactions. Figure 1 shows a schematic of the detector. It consists of two banks of six cylindrical NE213 liquid scintillators, each scintillator being 7.5 cm x 7.5 cm. The two banks are separated by 0.75m with a time-of-flight (TOF) system between the two banks to measure E_n', the scattered neutron energy. The principle of this mode of detection and the equations for energy and direction, E_n and θ_n, are included in the figure. All six detecting elements in each array, with accompanying photomultiplier tubes and high-voltage bleeders, are enclosed in an anti-coincidence shield.

The detector was used in a high-altitude balloon flight over Palestine, Texas. It was then in a complex flux of neutrons and gamma rays coming from all directions. Although the basic cross section, that for n-p scattering, and the basic geometry, as shown in the figure, are both well known, the complex radiation field and the uncertainty of corrections due to interactions with parts not shown in the figure leave one wanting empirically-determined efficiencies for at least a few values of E_n and θ_n. This was done for several values of θ_n at E_n=14 MeV (at N.H.), 28 MeV, and 42 MeV. These calibrations enabled us to normalize efficiencies obtained from a Monte Carlo calculation, which was then used to compute efficiencies for the data obtained in the balloon flight.

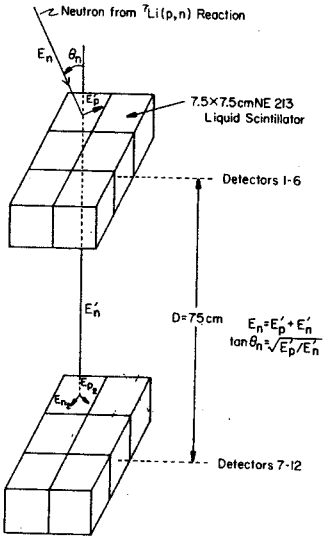

Fig. 1.-The detector system consists of 2 arrays, each of which holds six 7.5 cm x 7.5 cm cylindrical detectors. In addition, all detectors are surrounded by an anti-coincidence shield. For the event picture, E_p' is determined by the light collected from detector 1 while E_n' is obtained from the TOF over the 75 cm distance, allowing E_n and θ_n to be deduced from the formulas shown.

For the calibration at MSU the ^{7}Li(p,n)^{7}Be reaction was used to produce a known flux of neutrons on the detector. About one half of the neutrons produced at a forward angle in this reaction are concentrated in a narrow energy band at the top of the spectrum. In order to make the source more truly mono-energetic, the lower-energy neutrons were electronically eliminated by using a suitable time-of-flight gate. In order to prevent overlap of lower-energy neutrons from earlier proton beam bursts, the time between bursts was increased by transporting only every fourth burst from the cyclotron to the lithium target. The target thickness was determined, and for each run the proton beam charge was measured. When combined with the known energy and angle distribu-

tions of the $^{7}Li(p,n)$ reaction[4], we could then compute the absolute neutron flux to about ±15%. As a cross check we verified, by radioactive counting of one of the ^{7}Li targets, that the anticipated number of ^{7}Be atoms had been made.

1. S.F. Singer, Phys. Rev. Letters 1, 171 & 181 (1958).
2. J.A. Lockwood, C. Chen, L.A. Friling, and R.N. St. Onge, J. Geophys. Rec. 81, 6211 (1976).
3. J.A. Lockwood, C. Chen, L.A. Friling, D. Swarty, R. St. Onge, Aaron Galonsky, and R. R. Doering, Nucl. Instr. and Meth. 138, 353 (1976).
4. S.D. Schery, L.E. Young, R.R. Doering, Sam M. Austin, and R.K. Bhowmik, NIM (to be published).